Quantitative assessment in thermal image segmentation for artistic objects

Bardia Yousefi
Stefano Sfarra*
Xavier P. V. Maldague

Canada Research Chair in Multipolar Infrared : MiViM
Computer vision and systems laboratory, Department of Electrical and Computer Engineering,
Laval University, Quebec city, Canada

*University of **L'Aquila - Las.E.R. Laboratory - Department of Industrial and Information Engineering and Economics (DIIIE), Piazzale E.** Pontieri no. 1, I-67100, Monteluco di Roio, Roio Poggio - L'Aquila (AQ), Italy, European Union

UNIVERSITÉ LAVAL

MIVIM
Multipolar Infrared Vision

OUTLINE

INTRODUCTION

DETECTING DEFECT

RESULTS

CONCLUSION

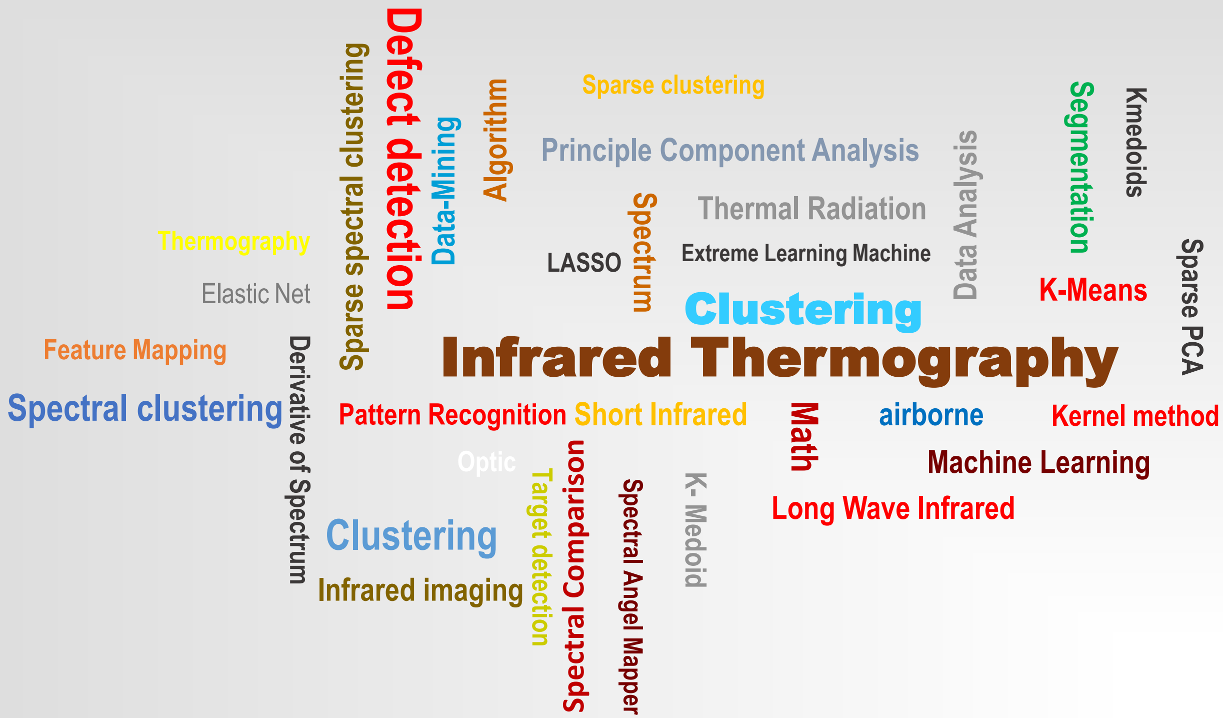

INTRODUCTION - Thermography

Infrared Non-Destructive Testing (IRNDT) provides thermographic images in the region of interest which usually involves defects.

Active thermography is a vast field including non-destructive and non-contact inspection techniques which have many applications in different industries

Applications

- Non-destructive Testing (NDT)
- Medical analysis (Computer Aid Diagnosis/Detection-CAD)
- Arts and Archaeology
- Geology
- Target detection
- *etc*

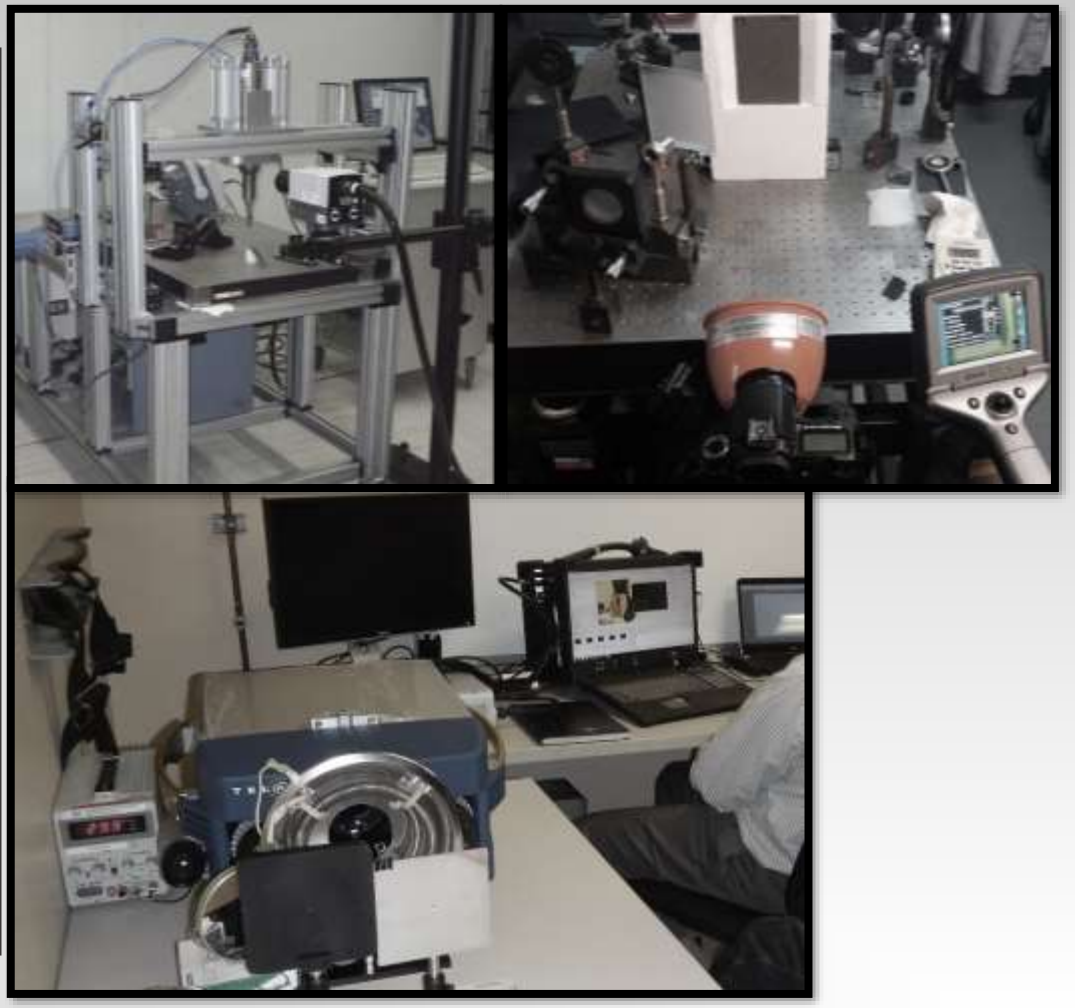

INTRODUCTION

- Segmentation by clustering

Segmentation approaches have been proposed for countless applications in different research areas such as NDT, thermal image analysis, etc.

Here the application of clustering in **segmentation of defects** is investigated.

Automatic defect detection helps to make our IRNDT system works:

- Faster
- More accurate
- More robust

Segmentation in Industrial, Art, and Archaeology Applications

Impacted on the composite

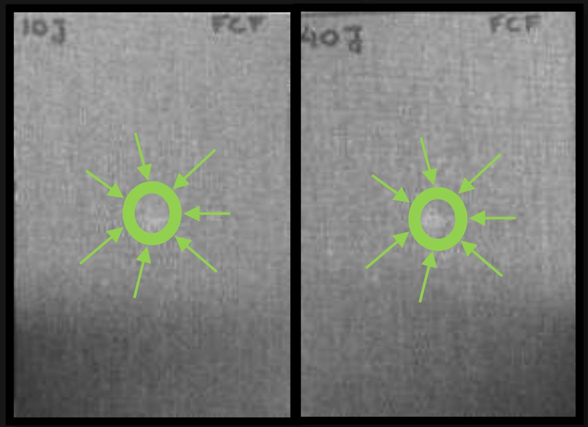

Fresco

Polychromatic wooden statue

INTRODUCTION

- Real examples of Segmentation

Application in Mineral identification using Hyperspectral infrared imagery

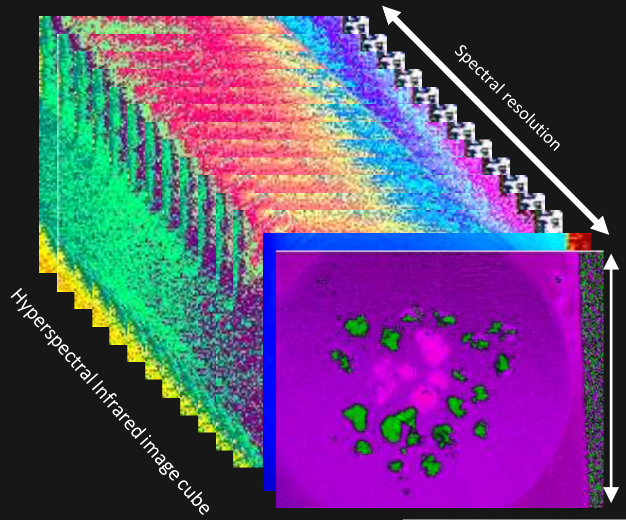

Long Wave Infrared Hyperspectral Thermography (7.7-11.8 µm)

Clustered false color images using color based K-means.

[1] Yousefi, B., Sojasi, S., Castanedo, C.I., Beaudoin, G., Huot, F., Maldague, X.P. and Chamberland, M. (2017). Hyperspectral Infrared Spectral Analysis for Automatic Identification of Mineral Grains. International Journal of Applied Earth Observation and Geoinformation, in press.

[2] Yousefi, B., Sojasi, S., Castanedo, C. I., Beaudoin, G., Huot, F., Maldague, X. P., ... & Lalonde, E. (2016, May). Mineral identification in hyperspectral imaging using Sparse-PCA. In SPIE Commercial+ Scientific Sensing and Imaging (pp. 986118-986118). International Society for Optics and Photonics.

Medical analysis Application

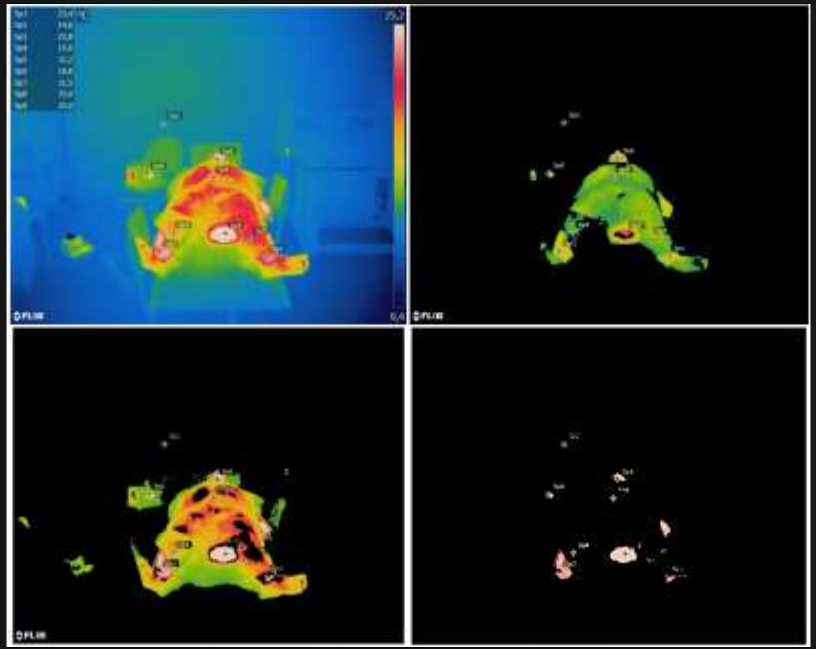

Results segmentation for different clusters showing different temperature

[3] Yousefi, B., Fleuret, J., Zhang, H., Maldague, X. P., Watt, R., & Klein, M. (2016). Automated assessment and tracking of human body thermal variations using unsupervised clustering. Applied Optics, 55(34), D162-D172.

These are the data analyzed under Canada research chair in infrared and thermography (MIVIM)

METHODOLOGY

- Our contribution

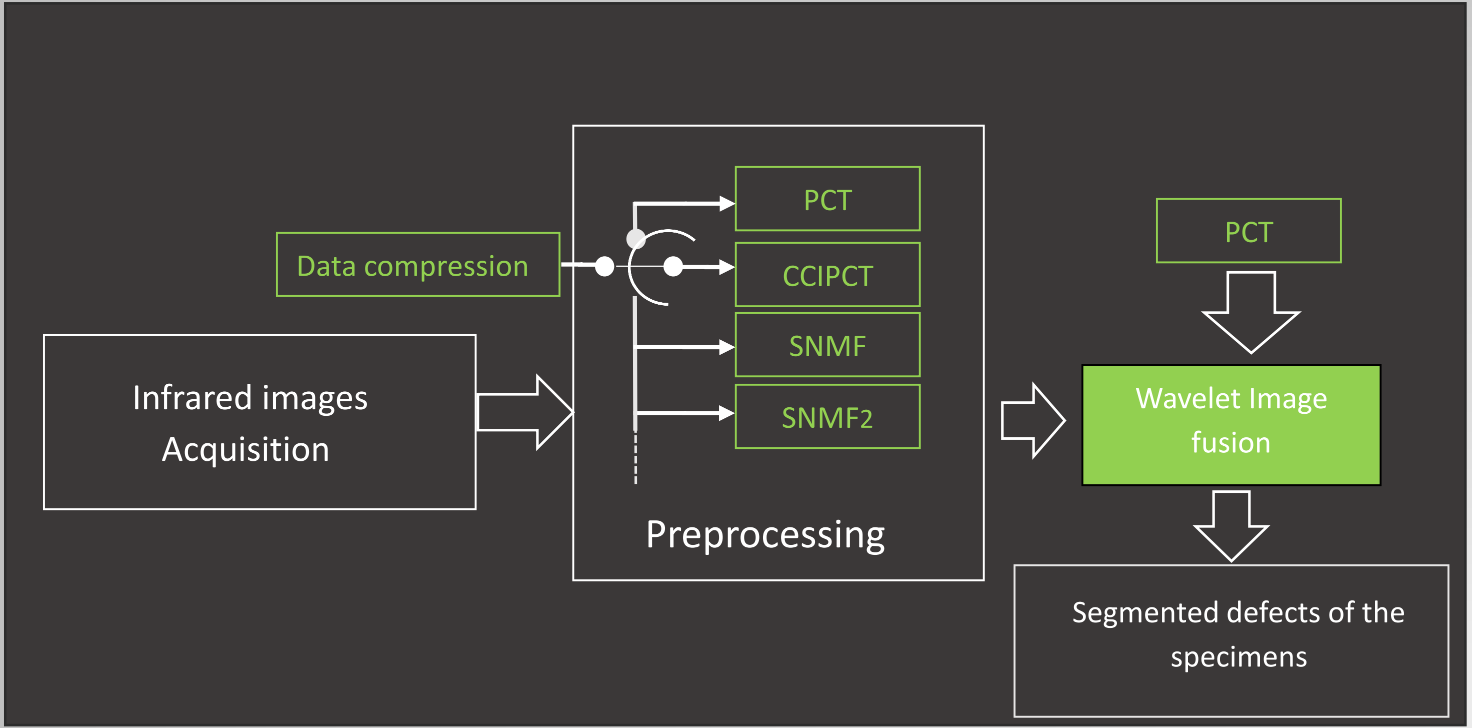

A good segmentation approach

A good segmentation approach is a powerful tool which uses in data-analysis and dataming. It provides numerous applications in different field.

Proposed Algorithm

Algorithm	
Given	Input data I(x,y,z) ∈ $\boldsymbol{R}^{N\times M\times Z}$ which I(x,y) ∈ $\boldsymbol{R}^{N\times M}$ is spatial dimension for infrared image selected and its unit is pixels, z represents the frequency of acquisition.
Step 1	Calculation of factor analysis $$\mathbf{M}_k\,(x,y) = FA_j\,(I(x,y,z))$$ $\boldsymbol{k}$ is number of the eigen-images taken selected for the analysis. $\boldsymbol{FA}$ presents the technique uses for decomposing the input data and j shows the types of techniques. $\boldsymbol{M_k(x,y)}$ shows the k[th] calculated eigen-image, $\boldsymbol{k < z}$.
Step 2	Selecting the best $\boldsymbol{M_{\acute{k}}(x,y)}$ amount the eigen-images. Let $\boldsymbol{\acute{k}}$ number of the best representative defect in images. $$\grave{\mathbf{M}}_{\acute{k}}(x,y,3) \xrightarrow{FC} M_{\acute{k}}(x,y)$$ Where $\grave{\mathbf{M}}_{\acute{k}}(x,y,3)$ shows the false color (FC) RGB matrix of $\boldsymbol{M_{\acute{k}}(x,y)}$.
Step 3	Clustering calculation for segmentation purpose. $$\grave{\mathbf{M}}_{\acute{k}}(x,y,3) \xrightarrow{HSV} X(a_i)_{i=1,2,3}$$ $$A(x,y,K) = min_{C,a_j} \sum_{c=1}^{K} \sum_{j=1}^{3} \lVert X(a_i) - m_c \rVert^2$$ $X(a_i)$ is shown the HSV color system matrix of $\grave{\mathbf{M}}_{\acute{k}}(x,y,3)$. Let $\boldsymbol{m_c}$ be the average value of data. $\mathbf{K}$ is shown the initial number of the clusters. Where the $\boldsymbol{A(x,y,K)}$ represents the segmented region.
Step 4	Calculating the second part of analysis using PCT: $$I(x,y,z) \xrightarrow{PCT} \Phi_\gamma(x,y)$$ $\boldsymbol{\Phi_\gamma(x,y)}$ shows the $\boldsymbol{\gamma^{th}}$ eigen-image of PCT which has the best representation of the defect. Applying defect's intensity level δ, the defect region can be found along with some false positive shown by $\boldsymbol{\Phi_\gamma^\delta(x,y)}$. δ obtained from $\boldsymbol{I(x,y,z')}$ $(z' \in \boldsymbol{R}^{Z'}, z \in \boldsymbol{R}^{Z}, Z' \Delta Z)$.
Output	Calculating Wavelet data fusion $$C(x,y) = \omega^{-1}\left[\phi\left(\omega[A(x,y,\dot{K})], \omega\left[\Phi_\gamma^\delta(x,y)\right]\right)\right]$$ Where $A\left(x,y,\dot{K}\right)$ is the best representative of defect through different $\dot{K} \le K$.

RESULTS

- Artistic objects

Location of the camera and heating sources

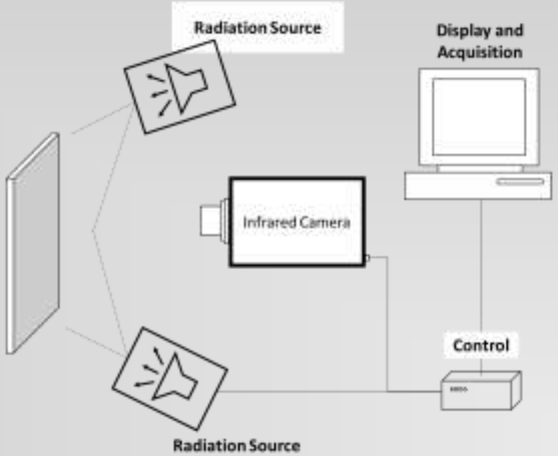

Scheme of the experimental setup

Child polychromatic wooden statue

The test conducted to gather the infrared images in the laboratory environment and the infrared vision experimental set up is shown in Figure. The infrared camera used was a long wave infrared camera (LWIR - 7.5–13 µm) having the spatial resolution of 240 *320 pixels. There were two radiation sources, i.e., two 250 W SICCATHERM E27 lamps that gave a wide radiation spectrum for thermography testing.

As the overheating is always a concern in artworks, the temperature of specimens were monitored during the test using a laser pyrometer. The temperature of the room was approximately 292K (19°C) at the starting of the thermographic inspection. During the test, the infrared thermography acquisition process was controlled using the spot function and the lamps were located far from the specimens (24 cm) to provide an adequate heating up phase. The distance lamp - lamp was 40 cm, while the thermal camera was put at 46 cm from the left cheek of the Child. The relative humidity(RH) was 47.5 % and the emissivity value was set at 0.90. The six hundred thermograms were reorded during 180 seconds of heating and seven minutes of cooling (420 thermograms).

RESULTS

- Artistic objects

Studied area of the Fresco (red line)

The system of thermal stimulation and acquisition for the sample – fresco

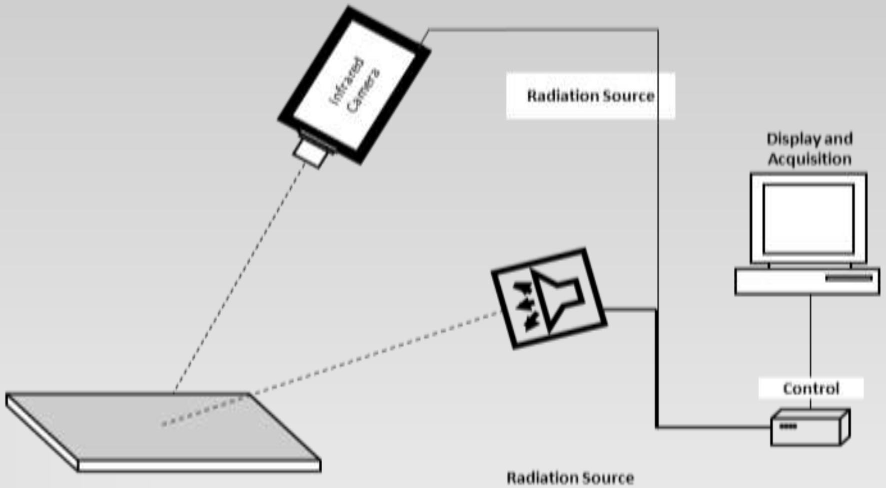

Scheme of the experimental setup of fresco

Real Fresco

In the experiment of the real fresco, the inspection by infrared reflectography (IRT) and the heating up phase lasted 360 seconds.. The camera located at $295 cm$ far from the sample and 1 lamp (2kW) at the distance of $235 cm$. The ambient temperature recorded was 16.2 °C, while the relative humidity was equal to 40.1%. Also in this case, the emissivity value was set at 0.90, although the new technique applied minimize the emissivity variation due to the pigments. The cooling down phase lasted 780 seconds, and 1 thermogram per second was recorded during the entire inspection procedure.

RESULTS

- Results of Child polychromatic wooden statue

a. Child polychromatic wooden statue

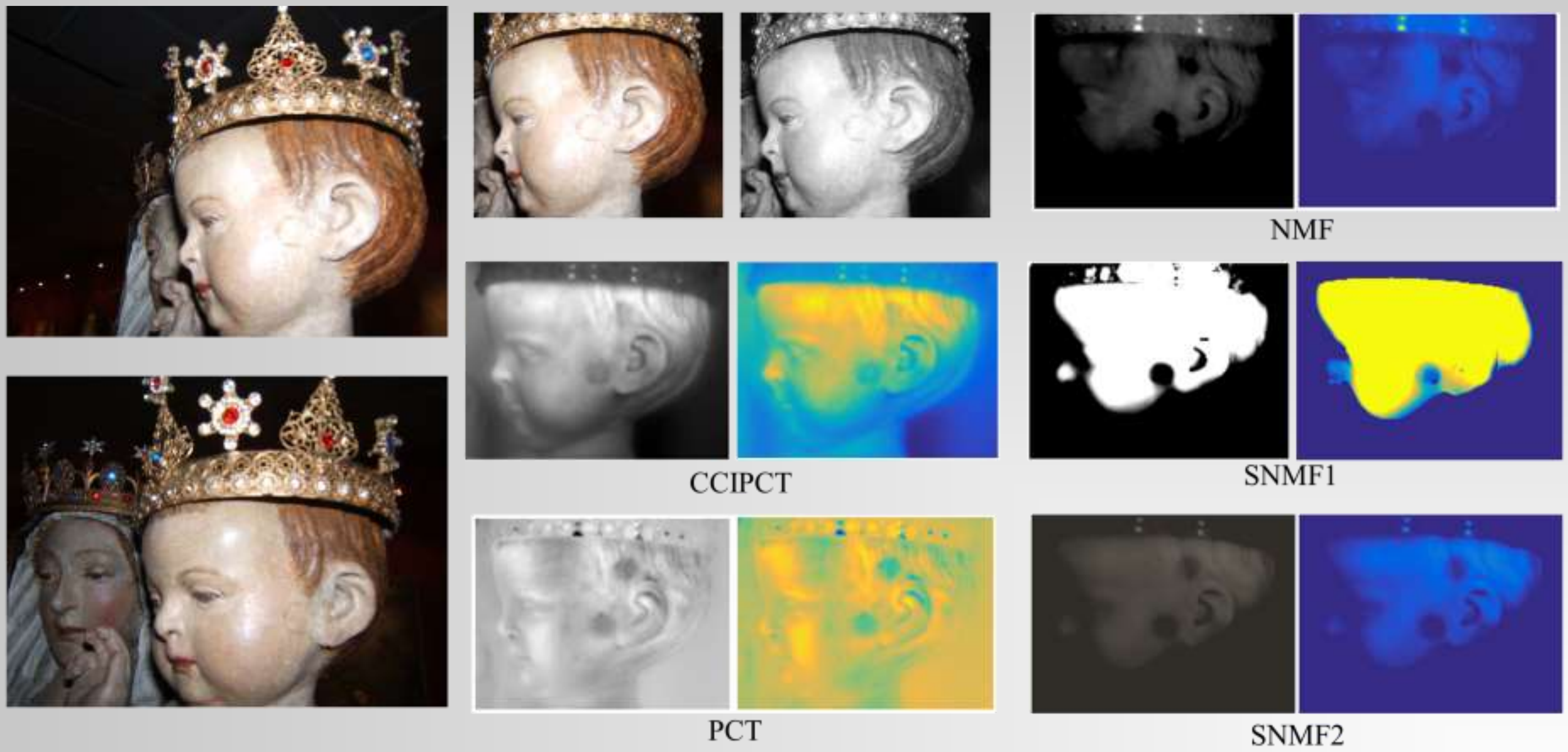

RESULTS

- Results of real Fresco

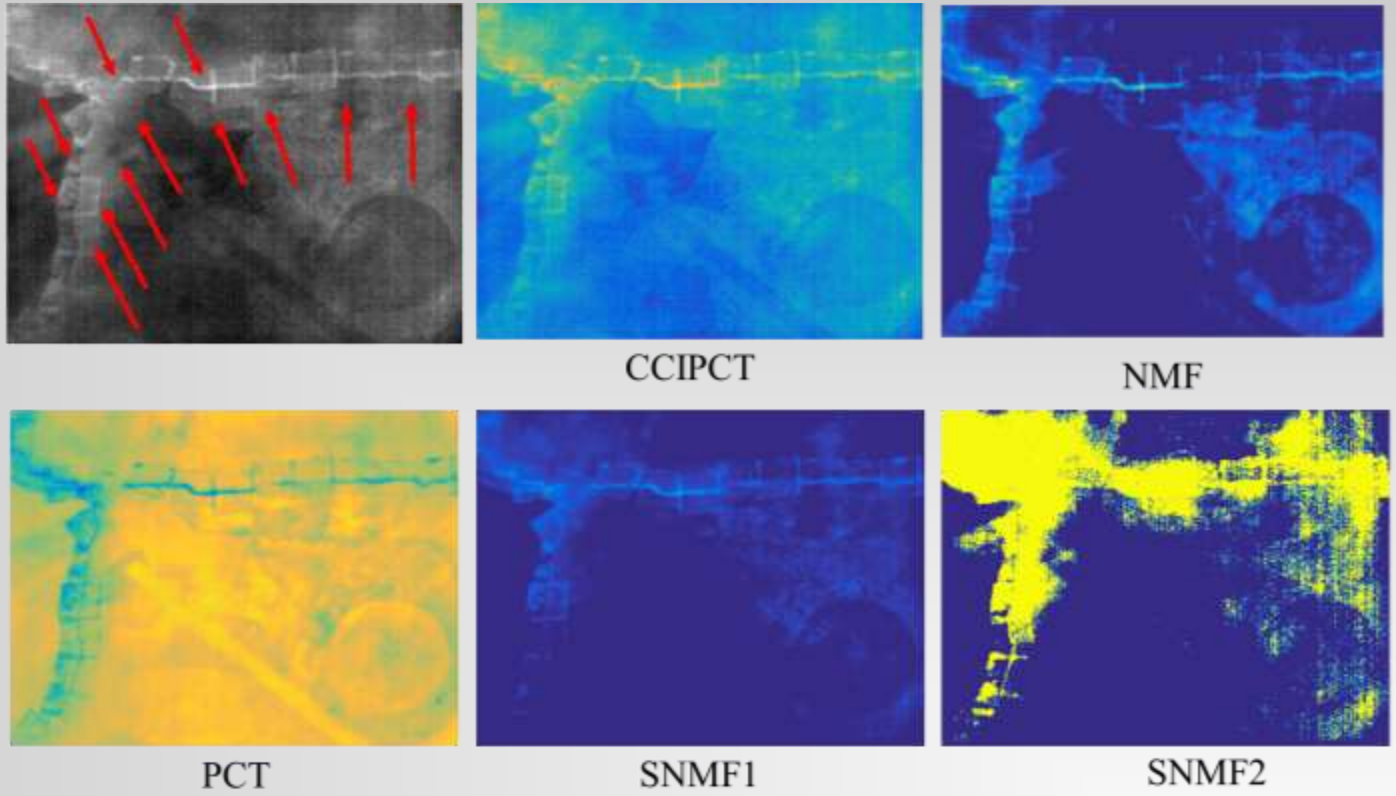

RESULTS

- Final segmentation

Automatic Detection of Defect in Art and Archaeology specimens

Polychromatic wooden statue[1]

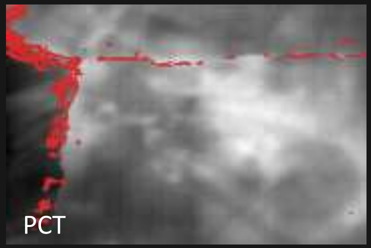

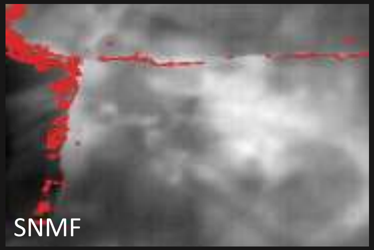

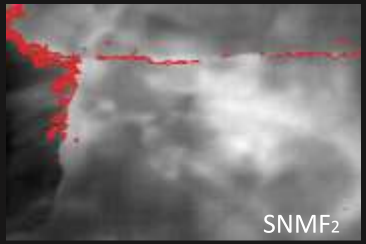

Fresco[1]

Principal Component Thermography (PCT)
Candid Covariance-Free Incremental Principal Component Thermography (CCIPCT)
Negative Matrix Factorization by gradient-descent-based multiplicative rules (SNMF)
Standard NMF by Non-negative least squares (NNLS) active-set algorithm (SNMF$_2$)

RESULTS

- Quantitative Results of Child polychromatic wooden statue

Child polychromatic wooden statue

The quantitative accuracy of our approach for the polychromatic statue is shown while we consider only one detected defect on the specimen surface.

Methods	Accuracy			
	Pixels corrected correctly	Accuracy (%)	False-positive	False-positive (%)
PCT	1292	100	387	29.9536
NMF	386	98.13	39	10.4558
CCIPCT	1445	100	10	0.6920
SNMF	551	99.81	0	0
SNMF2	983	100	70	7.12

The quantitative accuracy of our approach for the polychromatic statue is shown while we consider both defects on the specimen surface.

Methods	Accuracy					
	Pixels detected correctly	Accuracy (%)	False Negative	False Negative(%)	False-positive	False-positive (%)
PCT	2178	42.35	1841	35.79	17	0.3305
NMF	3627	70.52	423	8.2248	12	0.23
CCIPCT	1899	36.9240	3244	63.08	1536	29.87
SNMF	1355	26.3465	3538	68.7925	42	0.8166
SNMF2	3702	71.9813	718	13.9607	1050	20.4161

RESULTS

- Quantitative Results of real fresco

Real Fresco

The quantitative accuracy of our approach for the fresco is shown.

Methods	Accuracy					
	Pixels detected correctly	Accuracy (%)	False Negative	False Negative(%)	False-positive	False-positive (%)
PCT	3140	57.1013	42.8987	2359	3187	57.9560
NMF	3007	54.6827	45.3173	2492	2217	40.3164
CCIPCT	2890	52.5550	47.4450	2609	1770	32.1877
SNMF	3007	54.6827	45.3173	2492	2217	40.3164
SNMF2	2919	53.0824	46.9176	2580	1318	23.9680
Sparse PCT	2092	38.0433	61.9567	3407	936	17.0213

RESULTS

Computational time

Computational load

Table of computational cost for the proposed methods.

Methods	Computational load		
	Factor analysis (s)	Clustering (s)	Wavelet fusion (s)
PCT	1.570819	0.92	0.022
NMF	4.267770	0.72	0.02
CCIPCT	0.024910	1.19	0.021
SNMF	(for 1000 Iteration) 30.994544	0.84	0.018
SNMF2	(for 200 Iteration) 53.151630	0.722	0.032

Table of computational cost for the proposed methods for Fresco.

Methods	Computational load		
	Factor analysis (s)	Clustering (s)	Wavelet fusion (s)
PCT	9.678299	0.484188	0.011242
NMF	7.290876	2.285472	0.013743
CCIPCT	0.204019	0.112533	0.007896
SNMF	(for 1000 Iteration) 119.111053	0.169409	0.007228
SNMF2	(for 200 Iteration) 227.278529	0.092327	0.094902

CONCLUSIONS

- An algorithm for automatic detection of defect has been described.
- Two NDT for artistic samples (Child polychromatic wooden statue and real fresco) were used for benchmarking.
- Results of both samples have been shown.
- Computational complexity of the proposed algorithm has been estimated and quantitatively presented.

Future Work:

- Further investigate to test the approach for more samples and applications to verify its performance
- Further analysis to use more studies on clustering methods

THANK YOU

This research is done under Canada Research Chair in Multipolar Infrared : MiViM at Computer vision and systems laboratory (CVSL), Department of Electrical and Computer Engineering, Laval University, Quebec city, Canada

UNIVERSITÉ LAVAL

MIVIM

Multipolar Infrared Vision